Spinons and triplons in spatially anisotropic frustrated antiferromagnets

MASANORI KOHNO[1,2], OLEG A. STARYKH[3] AND LEON BALENTS[1]*

[1]Department of Physics, University of California, Santa Barbara, California 93106, USA
[2]Computational Materials Science Center, National Institute for Materials Science, Tsukuba 305-0047, Japan
[3]Department of Physics, University of Utah, Salt Lake City, Utah 84112, USA
*e-mail: balents@physics.ucsb.edu

Published online: 14 October 2007; doi:10.1038/nphys749

The search for elementary excitations with fractional quantum numbers is a central challenge in modern condensed-matter physics. It has long been speculated that two-dimensional frustrated magnets might support quantum disordered states with neutral spin-1/2 excitations known as spinons. Despite decades of search, however, no clear experimental examples have been found. We explore the possibility for several materials using a realistic model, the spin-1/2 spatially anisotropic frustrated Heisenberg antiferromagnet in two dimensions. Here, we derive an effective Schrödinger equation valid in the weak interchain coupling regime. The dynamical spin correlations from this approach agree quantitatively without fitting parameters with inelastic neutron measurements of the triangular antiferromagnet Cs_2CuCl_4. In such antiferromagnets, the spectrum is composed of an incoherent continuum arising from the effects of one-dimensional spinons of individual chains, and a sharp dispersing peak, due to coherently propagating 'triplon' bound states of two spinons. We argue that triplons are generic features of spatially anisotropic frustrated antiferromagnets, which arise because the bound spinon pair lowers its kinetic energy by propagating between chains.

The emergence of particles with fractional quantum numbers is known to be quite generic in one-dimensional (1D) conductors and magnets[1], for example, in 1D quantum wires and carbon nanotubes. The spin excitation carrying a fractional quantum number, spin 1/2, is referred to as a spinon[2,3]. In contrast, in dimensions higher than one, the elementary excitation above a magnetically ordered state is a magnon, which carries spin 1 (refs 4,5). Nevertheless, fractionalization has been repeatedly identified theoretically as a possible phenomenon underlying unusual experimental behaviour of strongly correlated materials in two and three dimensions and zero magnetic field, such as high-temperature superconductors, heavy fermions and frustrated quantum magnets. Resonating valence bond theories[6,7] and slave-particle approaches[8–10] have been developed to describe fractionalization in dimensions greater than one[11]. However, these approaches remain largely unproved. For decades, considerable effort has been devoted to the search for such exotic behaviours[12,13], and only recently, experimental indications of fractionalized particles[14,15] and disordered ground states[16–19] have been observed in some 2D frustrated antiferromagnets.

Here, we consider how spinons may appear in a 2D magnet as descendents of their 1D counterparts. Our focus is the spin-1/2 spatially anisotropic antiferromagnetic Heisenberg model defined by the following hamiltonian:

$$\mathcal{H} = \sum_{x,y} \left(J\mathbf{S}_{x+1,y} + J_1'\mathbf{S}_{x,y+1} + J_2'\mathbf{S}_{x+1,y+1} + J_3'\mathbf{S}_{x-1,y+1} \right) \cdot \mathbf{S}_{x,y}, \qquad (1)$$

where $\mathbf{S}_{x,y}$ is the spin-1/2 operator at site (x, y). Here, J denotes the intrachain coupling and J_1', J_2' and J_3' are interchain couplings as shown in Fig. 1. We take $J, J_1', J_2' > 0$, reflecting antiferromagnetic interactions, focusing on the frustrated case $J_1' = J_2' + J_3'$. The main result here is a physical picture of the magnetic excitations in this situation, which enables a parameter-free calculation of the inelastic magnetic structure factor $S(k, \omega)$ for the full range of energy transfers with ω varying from essentially zero to several times J. The result is valid provided only J_a'/J is not too large, and indeed reveals characteristic features of spinon excitations.

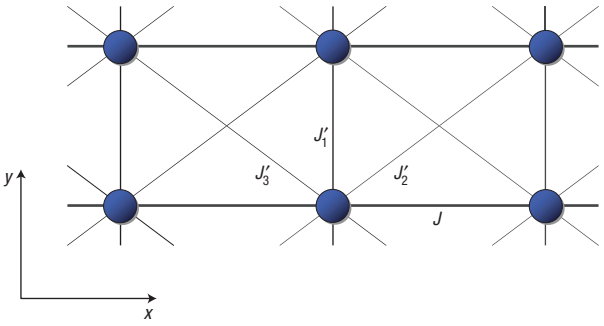

Figure 1 Lattice structure and coupling constants J_1', J_2', J_3' and J. The circles and lines denote sites and bonds, respectively.

One strong motivation to study this model comes from experiments on the material Cs_2CuCl_4, a spin-1/2 Heisenberg antiferromagnet on a spatially anisotropic triangular lattice. This corresponds to equation (1) with $J_1' = J_2' \equiv J'$ and $J_3' = 0$, and the measured anisotropy $J/J' \approx 3$ (ref. 20). The spectral weight in the measured dynamical structure factor, $S(k, \omega)$, is dominated by a broad continuum, extending up to energy above $3J$, with

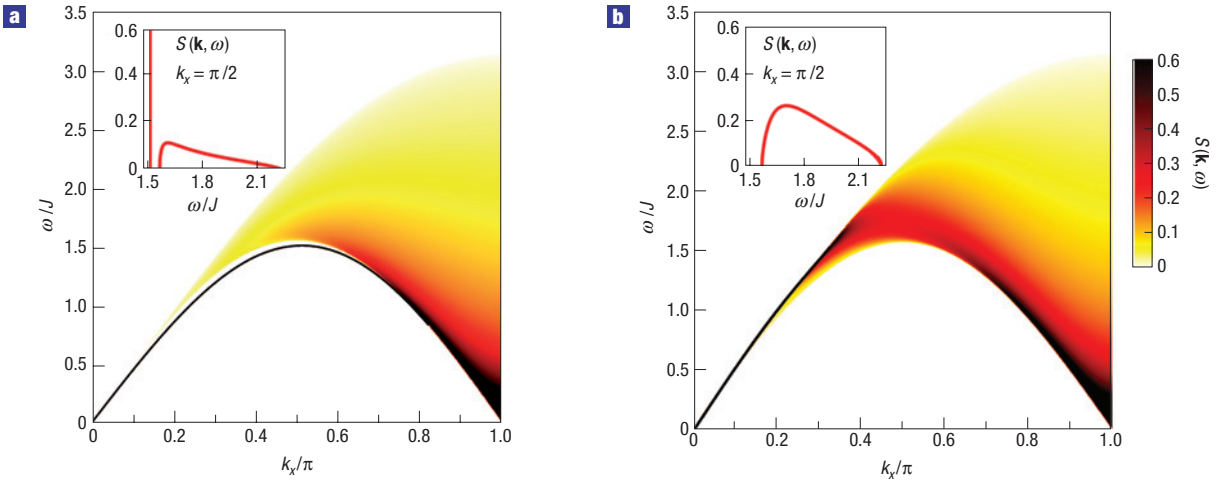

Figure 2 Dynamical structure factor $S(\mathbf{k},\omega)$ for $J'(\mathbf{k}) < 0$ and $J'(\mathbf{k}) > 0$. a,b, Density plot of $S(\mathbf{k},\omega)$ for $J'_2 = J'_3 = J'_1/2 = 0.24J$ at $k_y = \pi$ (**a**) and $k_y = 0$ (**b**). The insets show the plots at $k_x = \pi/2$.

the usually strong magnon peak appearing uncharacteristically insignificant. The spectral tail for some directions in momentum space is well fitted by a power-law form[14,15]. Following this observation, numerous theories have attributed the behaviour to fractionalized excitations of exotic 2D critical and/or spin-liquid states[21–26]. Other studies have compared the data with anharmonic spin-wave theory. The latter calculations reproduce the peak dispersion (but not the lineshape) in Cs_2CuCl_4, only, however, if the exchange parameters are substantially modified by hand[14,15,27,28]. Unbiased numerical series-expansion calculations do reproduce the peak dispersion quantitatively[29,30].

Here, we argue that the spectra in Cs_2CuCl_4 indeed reflect spinons as originally suggested, but that these spinons are descendents of the 1D excitations of the chains formed by the strong J bonds, and not characteristic of any exotic 2D state. A popular argument against this notion has been that the peak energy has substantial dispersion in the direction transverse to the chains. We show that contrary to naïve expectations, such dispersion does appear in a quasi-1D approach. The basic physics involved is the binding of two spinons into a delocalized and dispersing spin-1 pair (triplon). This is driven by kinetic energy, as only a pair of spinons may hop between chains. Triplon formation leads to specific signatures in the structure factor, which are indeed present in the data on Cs_2CuCl_4.

The appropriateness of the 1D approach is reinforced by several studies. Ref. 31 has quantitatively described most of the complex low-temperature phase diagram of Cs_2CuCl_4 in applied magnetic fields. It also showed that the frustrated J' coupling is ineffective in establishing long-range order: the characteristic energy scale for ordering is only of order $(J')^4/J^3$, much smaller than the bare interchain exchange J'. An early indication of this ineffectiveness appeared in ref. 32, in which a 'decoupled' state was suggested. More recently, the exact diagonalization study in ref. 33 found that correlations between spins in neighbouring chains remain extremely weak for $J' \leq 0.7J$.

This suggests that the elementary excitations (spinons) of independent spin chains are a natural basis. We therefore project the hamiltonian in equation (1) into the subspace of eigenstates of the 1D decoupled chains[34,35]. Each eigenstate can be characterized by the number of excited spinons, which is always even for any physical state. Remarkably, truncating to the first non-trivial approximation of only zero- or two-spinon states reproduces the main features of the spectrum of such quasi-1D frustrated antiferromagnets. Note that the two-spinon approximation is not a low-energy one (unlike the familiar and powerful 'bosonization' technique) as it includes spinons with energies reaching up to $\pi J/2 \gg J'$. This is essential for comparison with inelastic neutron scattering data which extends over this full range[15].

The two-spinon states of a single chain are characterized by two continuous quantum numbers, which can be thought of either as the momenta k_{x1}, k_{x2} of the individual (unbound) spinons, or equivalently, the total momentum $k_x = k_{x1} + k_{x2}$ and (excitation) energy $\epsilon = \epsilon_s(k_{x1}) + \epsilon_s(k_{x2})$ of the pair. We use the latter notation for convenience. The spinon energy follows the des Cloizeaux–Pearson dispersion, $\epsilon_s(k_x) = (\pi J/2)|\sin(k_x)|$ (ref. 36). The states can also be characterized by their total spin and S^z quantum numbers. Only the triplet ($s = 1$) states are relevant to the neutron structure factor, and we may specialize without loss of generality to the $S^z = +1$ state, which we denote $|k_x, \epsilon\rangle_y$ on chain y. For the many-chain system, the unperturbed ground state and two-spinon basis states are given as $|\mathrm{G.S.}\rangle_0 \equiv \otimes_y |0\rangle_y$ and $|k_x, \epsilon, y\rangle \equiv |k_x, \epsilon\rangle_y \otimes_{y' \neq y} |0\rangle_{y'}$, respectively. Here, $|0\rangle_y$ denotes the ground state of the y th Heisenberg chain, of length L_x.

We choose to work with eigenstates of the total 2D momentum vector $\mathbf{k} = (k_x, k_y)$. Such k_y eigenstates are superpositions: $|\epsilon\rangle_{\mathbf{k}} \equiv |k_x, k_y; \epsilon\rangle \equiv (1/\sqrt{L_y}) \sum_y e^{ik_y y} |k_x, \epsilon, y\rangle$ (here L_y is the number of chains). Note that because the two spinons comprising any of the original basis states always live in the same chain, there is only one intrinsic transverse momentum k_y and not two distinct spinon momenta in the y direction. Thus, there is only a one-parameter (ϵ) set of two-spinon states for each k_x, k_y. Therefore, the eigenstates in this basis take the form

$$|\Psi_{\mathbf{k}}\rangle = \int \mathrm{d}\epsilon \, D_{k_x}(\epsilon) \psi_{\mathbf{k}}(\epsilon) |\epsilon\rangle_{\mathbf{k}}, \qquad (2)$$

where $D_{k_x}(\epsilon) = \Theta(\omega_{2,u}(k_x) - \epsilon)\,\Theta(\epsilon - \omega_{2,l}(k_x))/\sqrt{\omega^2_{2,u}(k_x) - \epsilon^2}$ is the density of states of the Heisenberg chain, divided by $L_x/(2\pi)$, at momentum k_x and excitation energy ϵ (ref. 37) (Θ denotes the step function). It is restricted to $\omega_{2,l}(k_x) < \epsilon < \omega_{2,u}(k_x)$, where the boundaries of the two-spinon continuum are $\omega_{2,l}(k) = \epsilon_s(k_x)$ and $\omega_{2,u}(k_x) = \pi J \sin[k_x/2]$. The wavefunction $\psi_{\mathbf{k}}(\epsilon)$ defines the

spread of the eigenstate amongst this continuum. The condition that $|\Psi_{\mathbf{k}}\rangle$ is an eigenstate of the hamiltonian in the two-spinon subspace implies the Schrödinger equation:

$$\epsilon\psi_{\mathbf{k}}(\epsilon)+\int \mathrm{d}\tilde{\epsilon} D_{k_x}(\tilde{\epsilon})J'(\mathbf{k})A^{*}_{k_x}(\epsilon)A_{k_x}(\tilde{\epsilon})\psi_{\mathbf{k}}(\tilde{\epsilon})=E\psi_{\mathbf{k}}(\epsilon), \quad (3)$$

where E is the excitation energy above the ground state and $J'(\mathbf{k}) \equiv 2(J'_1\cos k_y + J'_2\cos(k_x+k_y) + J'_3\cos(k_x-k_y))$ is the Fourier transform of the interchain exchange interaction. The matrix element $A_{k_x}(\epsilon) \equiv (1/\sqrt{2})\langle 0|S^{-}_{-k_x,y}|k_x,\epsilon\rangle_y$, which is crucial for this study, was obtained exactly in ref. 38 (see the Supplementary Information).

We solved the integral equation, equation (3), numerically by carefully discretizing ϵ to obtain a complete (in the two-spinon subspace) set of eigenfunctions $\psi_{n\mathbf{k}}$ (and corresponding states $|\Psi_{n\mathbf{k}}\rangle$) and energies $E_{n\mathbf{k}}$, with $n=1,\ldots,M$. The number of discretized energies M was typically several thousand, as large as necessary to ensure good resolution. Knowing these eigenstates, we can directly evaluate the zero-temperature dynamical structure factor $S(\mathbf{k},\omega)$:

$$\begin{aligned} S(\mathbf{k},\omega) &= \int \frac{\mathrm{d}t}{2\pi}\mathrm{e}^{i\omega t}\langle \mathrm{G.S.}|S^{\alpha}_{-\mathbf{k}}(t)S^{\alpha}_{\mathbf{k}}(0)|\mathrm{G.S.}\rangle \\ &= \sum_n \left|\langle \mathrm{G.S.}|S^{\alpha}_{-\mathbf{k}}|\Psi_{n\mathbf{k}}\rangle\right|^2 \delta(\omega-E_{n\mathbf{k}}). \end{aligned} \quad (4)$$

For consistency, we approximate the ground state $|\mathrm{G.S.}\rangle$ by its perturbative form to first order in $J'(\mathbf{k})$, although this correction has little effect on the results. Details are given in the Supplementary Information.

Unexpectedly, it is possible to show analytically that the structure factor obtained in this way has nearly the same form as found in the well-known random phase approximation (RPA). In particular, as shown in the Supplementary Information (the $O(J')$ correction to the ground state is neglected for simplicity)

$$S(\mathbf{k},\omega)=\frac{S_{1\mathrm{D}}(k_x,\omega)}{[1+J'(\mathbf{k})\chi'_{1\mathrm{D}}(k_x,\omega)]^2+[J'(\mathbf{k})\chi''_{1\mathrm{D}}(k_x,\omega)]^2}. \quad (5)$$

Here $S_{1\mathrm{D}}(k_x,\omega)=\chi''_{1\mathrm{D}}(k_x,\omega)/\pi = D_{k_x}(\omega)|A_{k_x}(\omega)|^2$ is the two-spinon structure factor of a single chain[39] and $\chi'_{1\mathrm{D}}(k_x,\omega)=\int_0^{\infty}\mathrm{d}\omega' S_{1\mathrm{D}}(k_x,\omega')/(\omega'-\omega)$. This nearly coincides with the RPA expression, which is obtained by replacing our χ with the dynamic susceptibility of a single chain, $\chi'_{1\mathrm{D}}\to \mathrm{Re}\chi_{1\mathrm{D}}$, $\chi''_{1\mathrm{D}}\to \mathrm{Im}\chi_{1\mathrm{D}}$. $\mathrm{Re}\chi_{1\mathrm{D}}$ differs from $\chi'_{1\mathrm{D}}$ by a small contribution from $\omega'<0$. However, the differences between the RPA and our two-spinon result, with or without the ground-state correction, are very small in all situations of interest—see Supplementary Information.

We find three types of distinctive spectral feature depending on the momentum, determined by the value of $J'(\mathbf{k})$.

(1) $J'(\mathbf{k})<0$. $S(\mathbf{k},\omega)$ has a δ-function peak below the continuous spectrum. A typical example is shown in Fig. 2a. As discussed above, this peak arises from a triplon bound state of two spinons, $|\Psi_{1\mathbf{k}}\rangle$. The triplon dispersion $\omega_t(\mathbf{k})$ is determined from the pole of equation (5), where

$$1+J'(\mathbf{k})\chi'_{1\mathrm{D}}(k_x,\omega_t(\mathbf{k}))=0$$

and $\chi''_{1\mathrm{D}}(k_x,\omega_t(\mathbf{k}))=0$ outside the continuum. The pole appears below $\omega_{2,l}$ because there $\chi'_{1\mathrm{D}}$ is positive. The interchain dispersion of the triplon is due to the k_y dependence of $J'(\mathbf{k})$. In the weak interchain-coupling regime, the spectral weight Z and binding energy $\delta E=\omega_{2,l}(k_x)-\omega_t(\mathbf{k})$ of the peak are small, and behave as $Z\sim|J'(k_x,k_y)|$ and $\delta E\sim|J'(k_x,k_y)|^2$ (up to logarithmic corrections). See the Supplementary Information for details.

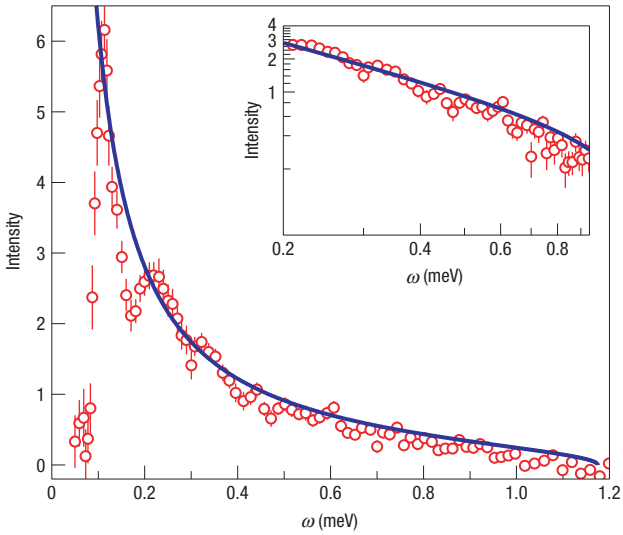

Figure 3 Comparison with the experimental result for dynamical structure factor $S(\mathbf{k},\omega)$ at $k'_x=\pi$. The solid line denotes the two-spinon structure factor $S_{1\mathrm{D}}(\pi,\omega)$ of a single chain with exchange $J=0.374$ meV (ref. 15). The symbols with error bars are the experimental data obtained by the inelastic neutron scattering experiment on Cs_2CuCl_4, taken from the G scan of Fig. 5 in ref. 15. The inset shows the log–log plot. The theoretical result is fitted to the experimental data by adjusting the height with a single multiplication factor.

(2) $J'(\mathbf{k})>0$. The spectral weight shifts upwards, and the peak is broadened in the continuum, see Fig. 2b. A suppression of spectral weight at the lower edge of the continuum occurs due to repulsion between the two spinons. When $J'(k_x,k_y)$ is sufficiently large, a δ-function peak appears above the two-spinon continuum. This peak corresponds to an anti-bound triplon state. However, the anti-bound peak is broadened by the four-spinon contribution, which leads to non-zero spectral density above the two-spinon upper boundary, $\omega>\omega_{2,u}$ (ref. 40).

(3) $J'(\mathbf{k})=0$. For such momenta, the structure factor is identical in the two-spinon approximation to that of a set of decoupled chains. For the frustrated situation of principal interest, where $J'_1=J'_2+J'_3$, this condition is always satisfied for $k_x=\pi$ (but it may also be true elsewhere).

Now, let us compare the above features with the experimental results[14,15] on Cs_2CuCl_4. The coupling constants are experimentally estimated as $J=0.374(5)$ meV and $J'=J'_1=J'_2=0.128(5)$ meV, which gives $J'/J=0.34(3)$ (ref. 20). This compound also has some very weak further Dzyaloshinskii–Moriya and interplane interactions not included in our model. The coupling constants of these interactions are experimentally estimated as about $0.05J$ (ref. 20). These are significant for the low-energy properties of the ordered phase[31,41] and excitations above it[42]. The ordering has negligible effect on the physics for energies higher than about $0.1J$, which is the regime of focus here and in the experiments in refs 14,15. In the notation of refs 14,15, the Fourier component of the interchain couplings reads $J'(\mathbf{k})=4J'\cos(k'_x/2)\cos(k'_y/2)$, where k'_x and k'_y are the momenta corresponding to the b and c axes in refs 14,15, respectively: $k'_x=k_x$ and $k'_y=k_x+2k_y$.

First, we discuss the large tail of $S(\mathbf{k},\omega)$ and the interpretation of the power-law behaviours observed in Cs_2CuCl_4 (ref. 15). In the present approach, a power-law behaviour at the lower edge of the continuum ($\omega_{2,l}$) is obtained only when $J'(\mathbf{k})=0$. There,

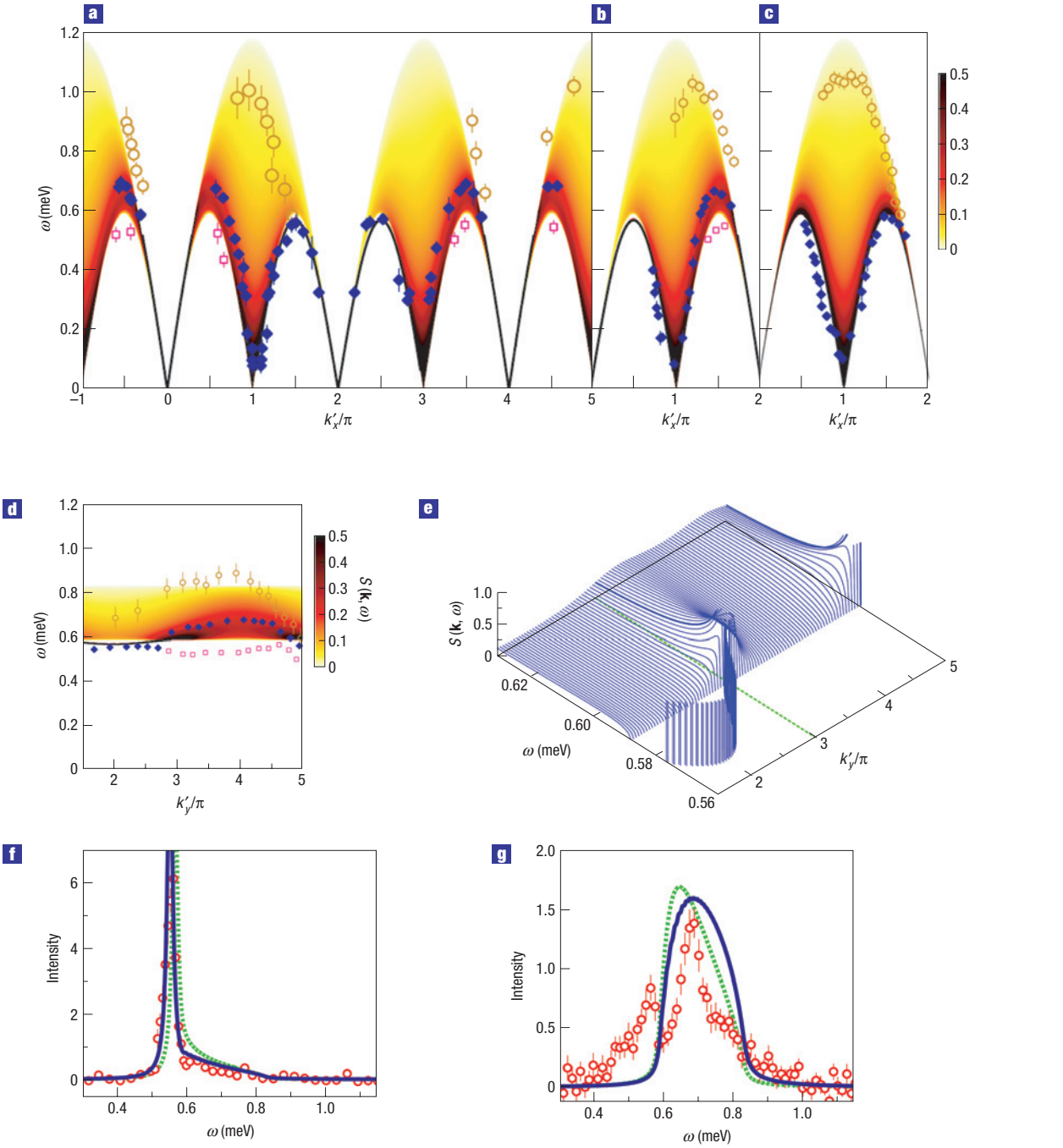

Figure 4 Comparison of $S(\mathbf{k}, \omega)$ with neutron scattering data on Cs_2CuCl_4. a–d, Comparison with experimental results for dispersion relations at $k'_y = 0$ (**a**), $k'_y = 2\pi$ (**b**), $k'_y = 3\pi$ (**c**) and $k'_x = -\pi/2$ (**d**). The density plots are the present results of dynamical structure factor $S(\mathbf{k}, \omega)$ for $J'_1 = J'_2 = 0.34J$, $J'_3 = 0$ and $J = 0.374$ meV. The filled and open symbols with error bars denote the main peak and the upper and lower edges of the spectrum observed by the neutron scattering experiment on Cs_2CuCl_4, respectively, taken from ref. 15. Graphs **a–d** correspond to (1), (3), (4) and (2) of Fig. 3 in ref. 15, respectively. **e**, $S(\mathbf{k}, \omega)$ at $k'_x = -\pi/2$ near the lower edge of continuum obtained by the present approach. The sign of $J'(\mathbf{k})$ changes at $k'_y = 3\pi$. **f**,**g**, Comparison with experimental data for the lineshape of $S(\mathbf{k}, \omega)$ at $\mathbf{k}' = (-\pi/2, 2\pi)$ (**f**) and $\mathbf{k}' = (-\pi/2, 4\pi)$ (**g**). The dotted lines are the present results within the two-spinon subspace multiplied by the normalization factor obtained by fitting the G scan in Fig. 3. The solid lines are the RPA result, which accounts for the four-spinon states as obtained in a chain of length $L_x = 288$, see the main text for the details. The numerical data in **f** and **g** are broadened by the energy resolution $\Delta E = 0.019$ meV of the spectrometer[15] including the isotropic magnetic form factor of Cu^{2+} ions. The symbols are experimental data for the E scan (**f**) and F scan (**g**) of Fig. 5 in ref. 15.

we expect the same behaviour as occurs in decoupled Heisenberg chains, that is, $S(\mathbf{k}, \omega) \propto \sqrt{-\ln[\omega - \omega_{2,l}]/[\omega - \omega_{2,l}]}$ at $k_x \neq \pi$ and $S(\mathbf{k}, \omega) \propto \sqrt{-\ln\omega}/\omega$ at $k_x = \pi$ near the lower edge of continuum[39]. On a spatially anisotropic triangular lattice, $J'(\mathbf{k})$ is zero on the lines of $k_x = \pi$ and $k_y = (\pi - k_x)/2$ in momentum space, which correspond to the lines of $k'_x = \pi$ and $k'_y = \pi$. The experimental

result at $k'_x = \pi$ is given as the G scan in ref. 15. The comparison of $S(\mathbf{k}, \omega)$ at $k'_x = \pi$ between the present result (that is, $S_{1D}(k, \omega)$ of the Heisenberg chain) and the experimental data (G scan in Fig. 5 of ref. 15) is shown in Fig. 3. Only a single fitting parameter—for the global height of intensity in this plot—has been used. For all further comparisons (below), we will use the same normalization, so the remaining comparisons are parameter-free. Although the theoretical curve and experimental data differ at low energies owing to the neglect of long-range magnetic order and the Dzyaloshinskii–Moriya interaction in the theory, the agreement at higher energy is quite good.

We next turn to the dispersion relation, which we define here, to ease comparison with experimental data, by the location of the peak $\omega(\mathbf{k})$ in $S(\mathbf{k}, \omega)$ at each $\mathbf{k}$. A comparison of our result and the experimental data (from Fig. 3 in ref. 15) is shown in Fig. 4. Note that there is no fitting parameter in this plot. The asymmetry of the dispersion relation of the main peak with respect to $k'_x = \pi$ and 3π observed at $k'_y = 0$ and 2π is consistently reproduced by the present approach (Fig. 4a,b). At $k'_y = 3\pi$, the dispersion relation is symmetric because $J'(\mathbf{k})$ is zero at this momentum, which is also consistent with the experimental observation (Fig. 4c). Despite the 1D starting point of the approach, it also explains the experimental dependence on transverse momentum (k'_y). Figure 4d,e shows $S(\mathbf{k}, \omega)$ in the perpendicular direction to k'_x at $k'_x = -\pi/2$. The sign of $J'(\mathbf{k})$ changes at $k'_y = 3\pi$. This causes the following change in $S(\mathbf{k}, \omega)$: as shown in Fig. 4e, a bound state is formed just below the continuum for $k'_y < 3\pi$. On the other hand, for $k'_y > 3\pi$, the spectral weight shifts upwards and the peak is broadened and absorbed into the continuum. Put simply, the lower edge of continuum (open squares in Fig. 4a–d) lies below the peak only in the region of $J'(\mathbf{k}) > 0$, and the main peak is always observed at the lowest energy of the spectrum for $J'(\mathbf{k}) \leq 0$. These features are exactly in accord with the theoretical predictions. Moreover, for $J'(\mathbf{k}) < 0$, the peak is much sharper (in fact resolution-limited) than for $J'(\mathbf{k}) > 0$. This is shown in Fig. 4f,g, which compares our theoretical predictions to scans E,F of ref. 15—note the factor of 3.5 larger scale in Fig. 4f compared with Fig. 4g.

Furthermore, the asymmetry of the experimental estimate of the upper edge of continuum with respect to $k'_x = \pi$ or $k'_y = 3\pi$ is also qualitatively understood: at the momenta with $J'(\mathbf{k}) > 0$, the spectral weight shifts upwards, and the high-energy weight becomes larger. On the other hand, in the region of $J'(\mathbf{k}) < 0$, the high-energy weight decreases, because part of it shifts into the bound state (Figs 2 and 4e). In agreement, the experiment (open circles in Fig. 4a–d) shows that the upper edge of continuum shifts a little bit along the momentum axis towards the region of $J'(\mathbf{k}) > 0$ from $k'_x = \pi$ or $k'_y = 3\pi$.

Our approach allows for systematic improvements by including further multi-spinon states. As a first step, we included the four-spinon states in the RPA approximation. This is done numerically by expressing the matrix element in equation (4) for a finite-length Heisenberg chain as a product of determinants[43–45]. The sum rule for the total spectral weight and the first frequency moment is satisfied by more than 99% for the length ($L_x = 288$) considered. We then calculate from this equation (5) using $\chi'_{1D} \rightarrow \mathrm{Re}\chi_{1D}$ and $\chi''_{1D} \rightarrow \mathrm{Im}\chi_{1D}$ and obtain the 2D $S(\mathbf{k}, \omega)$. We note that the finite-size errors for $L_x = 288$ are insignificant compared with the instrumental resolution. The resulting changes are small but very encouraging—the bound state in scan E has moved down a little, making agreement with experimental data essentially perfect (see Fig. 4f). We also observe that the anti-bound states, being located in the region of $\omega - \mathbf{k}$ space with non-zero spectral weight for four-spinon excitations, acquire a non-zero linewidth as expected, but that this is small enough that they remain visible features.

We conclude with a general discussion of our method and its ramifications. The most significant feature is the emergence of a spinon bound state driven by kinetic energy. Despite the superficial similarity to the more familiar magnon, the physics of the bound state is quite distinct. Specifically, a magnon is a Goldstone mode that emerges in a long-range ordered magnet as a consequence of broken symmetry. In our calculations, no such broken symmetry is presumed. Instead, the bound and anti-bound states are true $s = 1$ triplet excitations, better characterized as triplons than magnons[46,47].

Because in most cases, weakly coupled spin chains do eventually order at low enough temperature, it is important to understand the validity of our scheme in this situation. For this, it is crucial that we consider frustrated interchain couplings ($J'_1 = J'_2 + J'_3$). In this case, the leading divergence associated with coupling neighbouring chains—the strong tendency to Néel order at $k_x = \pi$ within each chain—is removed because $J'(\pi, k_y) = 0$. Without this condition, strong long-range Néel order which influences spectral features on the scale of $O(J')$ is obtained[48]. As this effect is comparable to those captured by the two-spinon approximation, the latter is unjustified without frustration. With frustration, any fluctuation-induced order has a much smaller characteristic energy scale[31,41,49], and can be neglected compared with the shifts of excited states captured by the present approach. Precisely this same frustration condition, $J'(\pi, k_y) = 0$, implies the persistence of 'free' spinons in the 2D neutron spectrum at these momenta. Of course, the presence of any long-range order, however weak, does modify some excitations in a qualitative manner. The triplon, when present, is expected to transform smoothly into a magnon as a consequence. In regions of momentum space where no bound state is present below the continuum, $J'(\mathbf{k}) > 0$, a magnon may weakly emerge as a consequence of long-range order.

There are numerous important directions for extensions and applications. It would be interesting to make a comparison with neutron measurements of Cs_2CuBr_4, which is isostructural to Cs_2CuCl_4 but with larger $J'/J \approx 0.5$ (ref. 50), and to search for signs of the anti-bound triplon in either material. Some theoretical extensions would be to include 3D and Dzyaloshinskii–Moriya couplings, to systematically treat higher-spinon states, to include thermal fluctuations at $T > 0$ and to take into account weak long-range order. A very interesting different direction is to apply analogous methods to spatially anisotropic strongly interacting conductors, modelled by Hubbard or t–J-type hamiltonians. Given the remarkable success of this approach in resolving the long-standing puzzle of the inelastic neutron spectra of Cs_2CuCl_4, and the very small arsenal of theoretical techniques capable of reliably obtaining intermediate energy spectra in strongly interacting systems above one dimension, further investigation of such methodology seems highly worthwhile.

Received 13 June 2007; accepted 12 September 2007; published 14 October 2007.

References

1. Haldane, F. D. M. 'Luttinger liquid theory' of one-dimensional quantum fluids. I. Properties of the Luttinger model and their extension to the general 1D interacting spinless Fermi gas. *J. Phys. C* **14**, 2585–2609 (1981).
2. Faddeev, L. D. & Takhtajan, L. A. What is the spin of a spin wave? *Phys. Lett. A* **85**, 375–377 (1981).
3. Haldane, F. D. M. "Spinon gas" description of the $S = 1/2$ Heisenberg chain with inverse-square exchange: Exact spectrum and thermodynamics. *Phys. Rev. Lett.* **66**, 1529–1532 (1991).
4. Anderson, P. W. An approximate quantum theory of the antiferromagnetic ground state. *Phys. Rev.* **86**, 694–701 (1952).
5. Kubo, R. The spin-wave theory of antiferromagnetics. *Phys. Rev.* **87**, 568–580 (1952).
6. Anderson, P. W. Resonating valence bonds: A new kind of insulator? *Mater. Res. Bull.* **8**, 153–160 (1973).
7. Kivelson, S. A., Rokhsar, D. S. & Sethna, J. P. Topology of the resonating valence-bond state: Solitons and high-T_c superconductivity. *Phys. Rev. B* **35**, 8865–8868 (1987).
8. Kotliar, G. & Ruckenstein, A. E. New functional integral approach to strongly correlated Fermi systems: The Gutzwiller approximation as a saddle point. *Phys. Rev. Lett.* **57**, 1362–1365 (1986).
9. Zou, Z. & Anderson, P. W. Neutral fermion, charge-e boson excitations in the resonating-valence-bond state and superconductivity in La_2CuO_4-based compounds. *Phys. Rev. B* **37**, 627–630 (1988).

10. Lee, P. A., Nagaosa, N. & Wen, X.-G. Doping a Mott insulator: Physics of high-temperature superconductivity. *Rev. Mod. Phys.* **78**, 17–85 (2006).
11. Senthil, T., Vishwanath, A., Balents, L., Sachdev, S. & Fisher, M. P. A. Deconfined quantum critical points. *Science* **303**, 1490–1494 (2004).
12. Kashima, T. & Imada, M. Magnetic and metal-insulator transitions through bandwidth control in two-dimensional Hubbard models with nearest and next-nearest neighbor transfers. *J. Phys. Soc. Jpn.* **70**, 3052–3067 (2001).
13. Morita, H., Watanabe, S. & Imada, M. Nonmagnetic insulating states near the Mott transitions on lattices with geometrical frustration and implications for κ-$(ET)_2Cu_2(CN)$. *J. Phys. Soc. Jpn.* **71**, 2109–2112 (2002).
14. Coldea, R., Tennant, D. A., Tsvelik, A. M. & Tylczynski, Z. Experimental realization of a 2D fractional quantum spin liquid. *Phys. Rev. Lett.* **86**, 1335–1338 (2001).
15. Coldea, R., Tennant, D. A. & Tylczynski, Z. Extended scattering continua characteristic of spin fractionalization in the two-dimensional frustrated quantum magnet Cs_2CuCl_4 observed by neutron scattering. *Phys. Rev. B* **68**, 134424 (2003).
16. Shimizu, Y., Miyagawa, K., Kanoda, K., Maesato, M. & Saito, G. Spin liquid state in an organic Mott insulator with a triangular lattice. *Phys. Rev. Lett.* **91**, 107001 (2003).
17. Helton, J. S. *et al.* Spin dynamics of the spin-1/2 kagome lattice antiferromagnet $ZnCu_3(OH)_6Cl_2$. *Phys. Rev. Lett.* **98**, 107204 (2007).
18. Ofer, O. *et al.* Ground state and excitation properties of the quantum kagomé system $ZnCu_3(OH)_6Cl_2$ investigated by local probes. Preprint at <http://arxiv.org/abs/cond-mat/0610540> (2006).
19. Masutomi, R., Karaki, Y. & Ishimoto, H. Gapless spin liquid behavior in two-dimensional solid ^{3}He. *Phys. Rev. Lett.* **92**, 025301 (2004).
20. Coldea, R. *et al.* Direct measurement of the spin hamiltonian and observation of condensation of magnons in the 2D frustrated quantum magnet Cs_2CuCl_4. *Phys. Rev. Lett.* **88**, 137203 (2002).
21. Chung, C. H., Marston, J. B. & McKenzie, R. H. Large-N solutions of the Heisenberg and Hubbard–Heisenberg models on the anisotropic triangular lattice: Application to Cs_2CuCl_4 and to the layered organic superconductors kappa-(BEDT-TTF)(2)X. *J. Phys. Condens. Matter* **13**, 5159–5181 (2001).
22. Zhou, Y. & Wen, X.-G. Quantum orders and spin liquids in Cs_2CuCl_4. Preprint at <http://arxiv.org/abs/cond-mat/0210662v3> (2002).
23. Chung, C. H., Voelker, K. & Kim, Y. B. Statistics of spinons in the spin-liquid phase of Cs_2CuCl_4. *Phys. Rev. B* **68**, 094412 (2003).
24. Yunoki, S. & Sorella, S. Resonating valence bond wave function for the two-dimensional fractional spin liquid. *Phys. Rev. Lett.* **92**, 157003 (2004).
25. Alicea, J., Motrunich, O. I. & Fisher, M. P. A. Algebraic vortex liquid in spin-1/2 triangular antiferromagnets: Scenario for Cs_2CuCl_4. *Phys. Rev. Lett.* **95**, 247203 (2005).
26. Isakov, S. V., Senthil, T. & Kim, Y. B. Ordering in Cs_2CuCl_4: Possibility of a proximate spin liquid. *Phys. Rev. B* **72**, 174417 (2005).
27. Veillette, M. Y., James, A. J. A. & Essler, F. H. L. Spin dynamics of the quasi-two-dimensional spin-1/2 quantum magnet Cs_2CuCl_4. *Phys. Rev. B* **72**, 134429 (2005).
28. Dalidovich, D., Sknepnek, R., Berlinsky, A. J., Zhang, J. & Kallin, C. Spin structure factor of the frustrated quantum magnet Cs_2CuCl_4. *Phys. Rev. B* **73**, 184403 (2006).
29. Zheng, W., Fjærestad, J. O., Singh, R. R. P., McKenzie, R. H. & Coldea, R. Anomalous excitation spectra of frustrated quantum antiferromagnets. *Phys. Rev. Lett.* **96**, 057201 (2006).
30. Fjærestad, J. O., Zheng, W., Singh, R. R. P., McKenzie, R. H. & Coldea, R. Excitation spectra and ground state properties of the layered spin-1/2 frustrated antiferromagnets Cs_2CuCl_4 and Cs_2CuBr_4. *Phys. Rev. B* **75**, 174447 (2007).
31. Starykh, O. A. & Balents, L. Ordering in spatially anisotropic triangular antiferromagnets. *Phys. Rev. Lett.* **98**, 077205 (2007).
32. Zheng, W., McKenzie, R. H. & Singh, R. R. P. Phase diagram for a class of spin-1/2 Heisenberg models interpolating between the square-lattice, the triangular-lattice, and the linear-chain limits. *Phys. Rev. B* **59**, 14367–14375 (1999).
33. Weng, M. Q., Sheng, D. N., Weng, Z. Y. & Bursill, R. J. Spin liquid phase in anisotropic triangular lattice Heisenberg model: Exact diagonalization and density-matrix renormalization group calculations. *Phys. Rev. B* **74**, 012407 (2006).
34. Bethe, H. Zur Theorie der Metalle. I. Eigenwerte und Eigenfunktionen der linearen Atomkette. *Z. Phys.* **71**, 205–226 (1931).
35. Hulthén, L. Über das Austauschproblem eines Kristalles. *Arkiv Mat. Astron. Fysik* **26A**, 1–106 (1938).
36. des Cloizeaux, J. & Pearson, J. J. Spin-wave spectrum of the antiferromagnetic linear chain. *Phys. Rev.* **128**, 2131 (1962).
37. Müller, G., Thomas, H., Beck, H. & Bonner, J. C. Quantum spin dynamics of the antiferromagnetic linear chain in zero and nonzero magnetic field. *Phys. Rev. B* **24**, 1429–1467 (1981).
38. Bougourzi, A. H., Couture, M. & Kacir, M. Exact two-spinon dynamical correlation function of the one-dimensional Heisenberg model. *Phys. Rev. B* **54**, R12669–R12672 (1996).
39. Karbach, M., Müller, G., Bougourzi, A. H., Fledderjohann, A. & Mütter, K.-H. Two-spinon dynamic structure factor of the one-dimensional $s = 1/2$ Heisenberg antiferromagnet. *Phys. Rev. B* **55**, 12510–12517 (1997).
40. Caux, J.-S. & Hagemans, R. The 4-spinon dynamical structure factor of the Heisenberg chain. *J. Stat. Mech.* P12013 (2006).
41. Bocquet, M., Essler, F. H. L., Tsvelik, A. M. & Gogolin, A. O. Finite-temperature dynamical magnetic susceptibility of quasi-one-dimensional frustrated spin-1/2 Heisenberg antiferromagnets. *Phys. Rev. B* **64**, 094425 (2001).
42. Essler, F. H. L., Tsvelik, A. M. & Delfino, G. Quasi-one-dimensional spin-1/2 Heisenberg magnets in their ordered phase: Correlation functions. *Phys. Rev. B* **56**, 11001 (1997).
43. Kitanine, N., Maillet, J. M. & Terras, V. Form factors of the XXZ Heisenberg spin-1/2 finite chain. *Nucl. Phys. B* **554**, 647 (1999).
44. Biegel, D., Karbach, M. & Müller, G. Transition rates via Bethe ansatz for the spin-1/2 planar *XXZ* antiferromagnet. *J. Phys. A* **36**, 5361 (2003).
45. Caux, J.-S., Hagemans, R. & Maillet, J. M. Computation of dynamical correlation functions of Heisenberg chains: The gapless anisotropic regime. *J. Stat. Mech.* P09003 (2005).
46. Damle, K. & Sachdev, S. Spin dynamics and transport in gapped one-dimensional Heisenberg antiferromagnets at nonzero temperatures. *Phys. Rev. B* **57**, 8307 (1998).
47. Schmidt, K. P. & Uhrig, G. S. Excitations in one-dimensional $S = 1/2$ quantum antiferromagnets. *Phys. Rev. Lett.* **90**, 227204 (2003).
48. Schulz, H. J. Dynamics of coupled quantum spin chains. *Phys. Rev. Lett.* **77**, 2790–2793 (1996).
49. Starykh, O. A. & Balents, L. Dimerized phase and transitions in a spatially anisotropic square lattice antiferromagnet. *Phys. Rev. Lett.* **93**, 127202 (2004).
50. Ono, T. *et al.* Magnetization plateaux of the $S = 1/2$ two-dimensional frustrated antiferromagnet Cs_2CuBr_4. *J. Phys. Condens. Matter* **16**, S773–S778 (2004).

Acknowledgements

We would like to thank J. Alicea, M. P. A. Fisher and R. Shindou for discussions. This work is supported by the Grant-in-aid for Scientific Research (C) No. 10354143 from MEXT, Japan (M.K.), the Petroleum Research Fund ACS PRF 43219-AC10 (O.S.), NSF grant/DMR-0457440 (L.B.) and the Packard Foundation (L.B.). Part of this research was completed at KITP and supported in part by the NSF under Grant No. PHY05-51164.
Correspondence and requests for materials should be addressed to L.B.
Supplementary Information accompanies this paper on www.nature.com/naturephysics.